Forecast system demonstrator

Deliverable ID:	**5.2**
Dissemination Level:	**PU**
Project Acronym:	**SINOPTICA**
Grant:	**892362**
Call:	**H2020-SESAR-2019-2**
Topic:	**SESAR-ER4-05-2019 - Environment and Meteorology for ATM**
Consortium Coordinator:	**CIMA Research Foundation**
Edition date:	**11 April 2022**
Edition:	**00.04.00**
Template Edition:	**02.00.02**

Co-funded by the European Union

EUROPEAN PARTNERSHIP

Authoring & Approval

Authors of the document

Name/Beneficiary	Position/Title	Date
Antonio Parodi/CIMA	Project Manager/Dr.	04/11/2021, 11/04/2022
Massimo Milelli/CIMA	Researcher/Dr.	11/11/2021
Riccardo Biondi/UNIPD	Project Communication Lead/Dr.	28/11/2021
Eugenio Realini/GRED	Project Quality Lead/Dr.	29/11/2021
Vincenzo Mazzarella	Researcher	16/01/2022
Laura Esbri	Researcher	23/02/2022

Reviewers internal to the project

Name/Beneficiary	Position/Title	Date
Eugenio Realini/GRED	Project Quality Lead/Dr.	29/11/2021
Riccardo Biondi/UNIPD	Project Communication Lead/Dr.	28/11/2021

Approved for submission to the SJU By - Representatives of beneficiaries involved in the project

Name/Beneficiary	Position/Title	Date
Antonio Parodi/CIMA	Project Manager/Dr	30/11/2021, 11/04/2022

Rejected By - Representatives of beneficiaries involved in the project

Name/Beneficiary	Position/Title	Date

Document History

Edition	Date	Status	Author	Justification
00.00.01	04/11/2021	First version	Antonio Parodi	
00.00.02	11/11/2021	Second version	Massimo Milelli	PHAST algorithm addition
00.00.03	27/11/2021	Third version	Antonio Parodi	Revision of the document
00.00.04	28/11/2021	Fourth version	Riccardo Biondi	Revision of the document
00.00.05	29/11/2021	Fifth version	Antonio Parodi	Revision of the document
00.00.06	29/11/2021	Sixth version	Eugenio Realini	Revision of the document
00.01.00	30/11/2021	Final version for submission	Antonio Parodi	
00.02.00	16/01/2022	Final version for submission	Vincenzo Mazzarella	Resubmission after SJU review
00.02.01	23/02/2022	Sevent version	Laura Esbrí, M. Carmen Llasat,	RaNDeVIL algorithm addition
00.03.00	28/02/2022	Final version for submission	Antonio Parodi	Final cleanup of the document
00.04.00	11/04/2022	Ready for submission	Antonio Parodi	Implemented comments by SJU reviewers

Copyright Statement

Co-funded by the European Union

EUROPEAN PARTNERSHIP

SINOPTICA

SATELLITE-BORNE AND IN-SITU OBSERVATIONS TO PREDICT THE INITIATION OF CONVECTION FOR ATM

This Report about Forecast system experiments (D5.2) is part of a project that has received funding from the SESAR Joint Undertaking under grant agreement No 892362 under European Union's Horizon 2020 research and innovation programme.

Abstract

The deliverable concerns the description of the tools used for the achievement of the project's objectives. In detail, the meteorological model Weather Research and Forecasting (WRF) is described, with a general overview followed by a description of its main physical parametrizations. Moreover, the nowcasting algorithms PhaSt and RaNDeVIL are introduced and presented.

Co-funded by the European Union

EUROPEAN PARTNERSHIP

Table of Contents

List of Tables

None

List of Figures

Co-funded by the European Union

EUROPEAN PARTNERSHIP

1 Introduction

This deliverable presents the three modelling tools adopted in this project, namely the Weather Research and Forecasting (WRF) Model, the "Phase Stochastic" (PhaSt) and RaNDeVIL nowcasting techniques.

These modelling tools will be applied to the SINOPTICA case studies (deliverable D5.1) and the related results presented in D5.3.

1.1 Acronyms and Terminology

Acronym	Description
ARW	Advanced Research version of WRF
DM	Double Moment
DVIL	Density of the Vertical Integrated Liquid
ETM	Echo Top in metre
YSU	Yonsei University
LES	Large Eddy Simulation
LSM	Land-Surface Models
MLCAPE	Mixed Layer Convective Available Potential Energy
MRF	Medium Range Forecast
NOAA	National Oceanic and Atmospheric Administration
PBL	Planetary Boundary Layer
PhaSt	Phase Stochastic
RaNDeVIL	Radar Nowcasting Density of the Vertical Integrated Liquid
RRTMG	Rapid Radiative Transfer Model for GCMs
RUC	Rapid Update Cycle
VIL	Vertically Integrated Liquid
VMI	Vertical Maximum Intensity
WRF	Weather Research and Forecasting Model

Co-funded by the European Union
EUROPEAN PARTNERSHIP

1.2 WRF model

The Weather Research and Forecasting (WRF) Model is a next-generation mesoscale numerical weather prediction system designed to serve both operational forecasting and atmospheric research needs.

At the end of the last century, around 1995, the United States' National Centers for Environmental Prediction (NCEP) had interest in developing a nonhydrostatic model for operational forecasting on finer scales. This idea arose on the premise that a numerical weather prediction (NWP) model shared between research and operational sector could have led to a beneficial synergy for both communities since the model could be a common platform on which an extensive research community develop capabilities that operatives could really exploit.

The original partners to build WRF were NCAR, the National Oceanic and Atmospheric Administration (NOAA), the U.S. Air Force, the Naval Research Laboratory, the University of Oklahoma, and the Federal Aviation Administration. The first model release at the end of December 2000 emerged from the partners' efforts was a model with a higher-order numerical accuracy and scalar conservation properties than the previous models such as the fifth-generation Pennsylvania State University–NCAR Mesoscale Model (MM5; [1]) developed during the 1990s. The model contained a preprocessor for domain and input preparation, an evolution of an initial physical packages ported from the MM5 and two alternative atmospheric fluid flow solvers or cores. The two WRF variants were called the Advanced Research version of WRF (ARW) WRF-ARW and the NCEP's Nonhydrostatic Mesoscale Model (NMM) WRF-NMM. Oversight of the WRF enterprise has evolved over time. Through the early years, the partners coordinated the various efforts and at the developmental level, various working groups focused on narrower areas, such as numerics, data assimilation, and physics. From the late 2000s, the original top-down direction of WRF has transitioned to a mode of community-driven input, with the responsibility for basic system and community support led by NCAR.

The WRF simulations are produced by two phases, the first to configure the model domain(s), ingest the input data, and prepare the initial conditions, and the second to run the forecast model and this is done by the forecast component that contains the dynamical solver and physics packages for atmospheric processes (e.g., microphysics, radiation, planetary boundary layer). The forecast model components operate within WRF's software framework, which handles I/O and parallel-computing communications. WRF is written primarily in Fortran, can be built with several compilers, and runs predominately on platforms with UNIX-like operating systems, from laptops to supercomputers. WRF model is applied extensively under both real-data and idealized configuration for research activity, but it is also used operationally at governmental centers around the world as well as by private companies.

WRF is suitable for a broad spectrum of applications across scales ranging from meters to thousands of kilometers and has been widely used by the proposers for hydro-meteorological research applications [2],[3],[4],[5],[6],[7],[8],[9].

The WRF model represents the atmosphere with several variables of state discretized over regular Cartesian grids. The model solution is computed using an explicit high-order Runge-Kutta timesplit integration scheme [10] in the two horizontal dimensions with an implicit solver in the vertical. Since WRF domains are decomposed over processors in the two horizontal dimensions only, inter-process communication is between neighbors on most supercomputer topologies. Each time-step involves 36 halo exchanges and a total of 144 nearest-neighbor exchanges (assuming aggregation). The decomposition is two-levels: first over distributed memory patches and then again within each patch

Co-funded by the European Union
EUROPEAN PARTNERSHIP

over shared memory tiles. Thus, WRF exploits hybrid parallel (message passing and multi-threaded) computation modes. Weather prediction codes are I/O (mostly output) intensive. WRF uses Parallel NetCDF for I/O. The WRF Data Assimilation system (WRFDA, formerly known as WRF-VAR) is a unified (global/regional, multi-model, 3/4D-Var) model-space data assimilation system.

1.2.1 WRF surface parameterizations

This paragraph presents general concepts about WRF surface schemes for numerical weather prediction including planetary boundary layer, atmospheric surface layer, and land surface model components (Figure 1).

The planetary boundary layer (PBL) is the lowest part of the atmosphere. Its behavior is directly influenced by its contact with a planetary surface. On Earth it usually responds to changes in surface radiative forcing in an hour or less. In this layer, physical quantities such as flow velocity, temperature, moisture, etc., display rapid fluctuations (turbulence) and vertical mixing is strong. Above the PBL is the "free atmosphere" where the wind is approximately geostrophic (parallel to the isobars) while within the PBL the wind is affected by surface drag and turns across the isobars. The free atmosphere is usually nonturbulent, or only intermittently turbulent.

The atmospheric surface layer is the lowest part of the PBL (typically about a tenth of the height of the PBL) where mechanical (shear) generation of turbulence exceeds buoyant generation or consumption. Turbulent fluxes and stress are nearly constant with height in this layer.

The earth/land (land hereafter) surface layer involves several crucial processes for “free” atmosphere and PBL namely infiltration, internal soil moisture fluxes, internal soil heat fluxes, and gravitational flow.

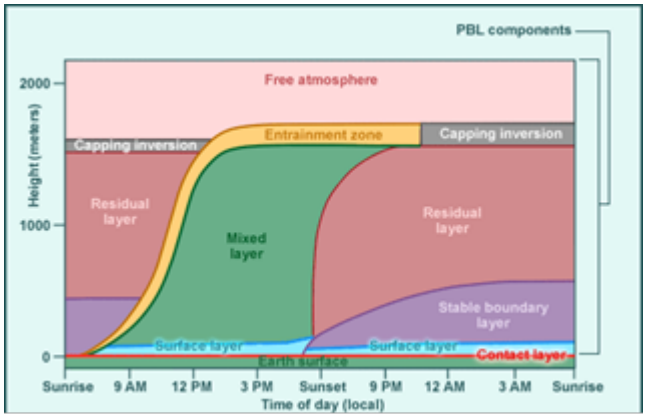

Figure 1: planetary boundary layer, and atmospheric surface layer daily cycle.

The PBL, the atmospheric surface layer and the land surface layer interact through some key processes (Figure 2): the atmospheric surface layer provides exchange coefficients for heat and moisture to the land surface layer, while the land surface layer provides land-surface fluxes of heat and moisture to the PBL, and finally the atmospheric surface layer supplies friction stress and water-surface fluxes of heat and moisture to the PBL.

Co-funded by the European Union
EUROPEAN PARTNERSHIP

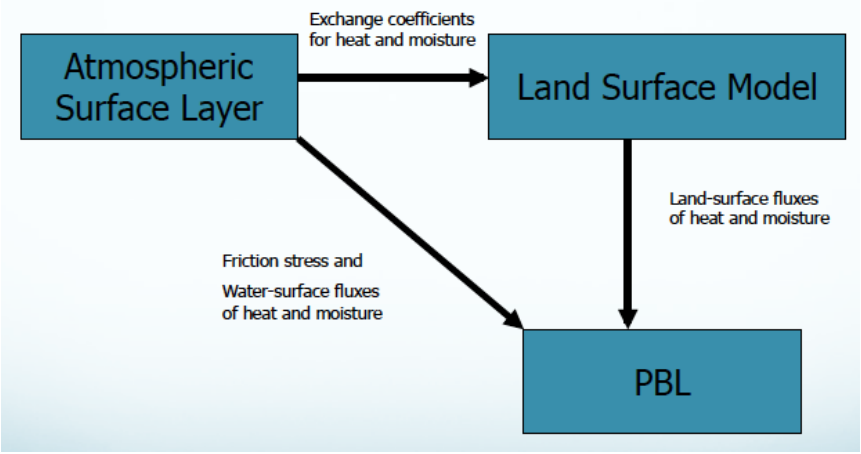

Figure 2: main interactions between planetary boundary layer, the atmospheric surface layer and the land surface layer.

Surface processes are dealt in WRF model through a set of physics categories which are summarized as planetary boundary layer and land-surface parameterizations, discussed hereafter. The adopted parameterizations for the SINOPTICA project simulations will be discussed hereafter.

1.2.2 The surface Layer

The surface layer schemes calculate friction velocities and exchange coefficients that enable the calculation of surface heat and moisture fluxes by the land-surface models and surface stress in the PBL scheme. Over water surfaces, the surface fluxes and surface diagnostic fields are computed in the surface layer scheme itself. The schemes provide no tendencies, only the stability-dependent information about the surface layer for the land-surface and PBL schemes. Some boundary layer schemes require the thickness of the surface layer in the model to be representative of the actual surface layer (e.g., 50-100 meters).

In this project we adopted the MM5 scheme, using the stability functions from [11], [12] to compute surface exchange coefficients for heat, moisture, and momentum. A convective velocity following [13] is used to enhance surface fluxes of heat and moisture. No thermal roughness length parameterization is included in the current version of this scheme. A Charnock relation relates roughness length to friction velocity over water. There are four stability regimes following [14].

1.2.3 The Land-Surface Model

The Land-Surface Models (LSMs) use atmospheric information (Figure 3) from the surface layer scheme, radiative forcing from the radiation scheme, precipitation forcing from the microphysics and convective schemes, surface temperature, water vapor and wind from the PBL scheme, together with internal information on the land's state variables and land-surface properties, to provide heat and moisture fluxes over land points and sea-ice points.

Co-funded by the European Union
EUROPEAN PARTNERSHIP

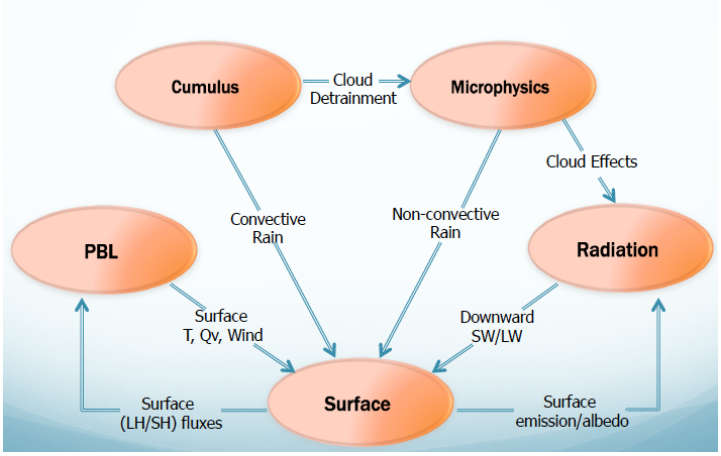

Figure 3: direct interactions of parameterizations, with special focus on surface related ones.

These fluxes provide a lower boundary condition for the vertical transport done in the PBL schemes (or the vertical diffusion scheme in the case where a PBL scheme is not run, such as in large-eddy mode). The LSMs have various degrees of sophistication in dealing with thermal and moisture fluxes in multiple layers of the soil and may handle vegetation, root, and canopy effects and surface snow-cover prediction. The LSM provides no tendencies but does update the land's state variables which include the ground (skin) temperature, soil temperature profile, soil moisture profile, snow cover, and possibly canopy properties. There is no horizontal interaction between neighboring points in the LSM, so it can be regarded as a one-dimensional column model for each WRF land grid-point, and many LSMs can be run in a stand-alone mode.

In this project we used the Rapid Update Cycle (RUC) LSM which has a multi-level soil model (6 levels is default but it could be set up to 9) with higher resolution in the top part of soil domain (0, 5, 20, 40, 160, 300 cm is default). The soil model solves heat diffusion and Richards moisture transfer equations, and in the cold season considers phase changes of soil water [15], [16]. The RUC LSM also has a multi-layer snow model with changing snow density, refreezing liquid water percolating through the snowpack, snow depth and temperature dependent albedo, melting algorithms applied at both snow-atmosphere interface and snow-soil interface, and simple parameterization of fractional snow cover with possibility of grid averaged skin temperature going above freezing. It also includes vegetation effects and canopy water. The RUC LSM has a layer approach to the solution of energy and moisture budgets. The layer spans the ground surface and includes half of the first atmospheric layer and half of the top soil layer with the corresponding properties (density, heat capacity, etc.). The residual of the incoming fluxes (net radiation, latent and sensible heat fluxes, soil heat flux, precipitation contribution into heat storage, etc.) modify the heat storage of this layer. An implicit technique is applied to the solution of these equations. Prognostic variables include soil temperature, volumetric liquid, frozen and total soil moisture contents, surface and sub-surface runoff, canopy moisture, evapotranspiration, latent, sensible and soil heat fluxes, heat of snow-water phase change, skin temperature, snow depth and density, and snow temperature.

Co-funded by the European Union
EUROPEAN PARTNERSHIP

1.2.4 The Planetary boundary layer Model

In the set of equation for turbulent flow the number of unknowns is larger than the number of equations, therefore there are unknown turbulence terms which must be parameterized as a function of known quantities and parameters. Much of the problem in numerical modeling of the turbulent atmosphere is related to the numerical representation (or parameterization as a function of known quantities and parameters) of these fluxes. This problem is known as closure problem. Closure can be local and non-local: for local closure, an unknown quantity in any point in space is parameterized by values and/or gradients of known quantities at the same point; for non-local closure, an unknown quantity at one point in space is parameterized by values and/or gradients of known quantities at many points in space; additionally the use of first-order closure schemes for evaluating turbulent fluxes is common in many boundary layer, mesoscale, and general circulation models of the atmosphere.

In this framework, the PBL model/parameterization is responsible for vertical sub-grid-scale fluxes due to eddy transports in the whole atmospheric column, not just the boundary layer. Thus, when a PBL scheme is activated, explicit vertical diffusion is de-activated with the assumption that the PBL scheme will handle this process. The most appropriate horizontal diffusion choices are those based on horizontal deformation or constant horizontal diffusion values, where horizontal and vertical mixing are treated independently. The surface fluxes are provided by the surface layer and land-surface schemes. The PBL schemes determine the flux profiles within the well-mixed boundary layer and the stable layer, and thus provide atmospheric tendencies of temperature, moisture (including clouds), and horizontal momentum in the entire atmospheric column. Most PBL schemes consider dry mixing but can also include saturation effects in the vertical stability that determines the mixing. The schemes are one-dimensional and assume that there is a clear scale separation between sub-grid eddies and resolved eddies. This assumption will become less clear at grid sizes below a few hundred meters (Large Eddy Simulation, LES, mode), where boundary layer eddies may start to be resolved, and in these situations the scheme should be replaced by a fully three-dimensional local sub-grid turbulence scheme.

WRF PBL schemes can be:

- based on turbulent kinetic energy prediction
- diagnostic non-local

The scheme adopted in the project is the Yonsei University (YSU) PBL [17], which is the next generation of the Medium Range Forecast (MRF) PBL, also using the counter gradient terms to represent fluxes due to non-local gradients. This adds to the MRF PBL [18] an explicit treatment of the entrainment layer at the PBL top. The entrainment is made proportional to the surface buoyancy flux in line with results from studies with large-eddy models [19]. The PBL top is defined using a critical bulk Richardson number of zero (compared to 0.5 in the MRF PBL), so is effectively dependent on the buoyancy profile, in which the PBL top is defined at the maximum entrainment layer (compared to the layer at which the diffusivity becomes zero). A smaller magnitude of the counter-gradient mixing in the YSU PBL produces a well-

Co-funded by the European Union
EUROPEAN PARTNERSHIP

mixed boundary-layer profile, whereas there is a pronounced over-stable structure in the upper part of the mixed layer in the case of the MRF PBL. Details are available in [17], including the analysis of the interaction between the boundary layer and precipitation physics. In version 3.0, an enhanced stable boundary-layer diffusion algorithm [20] is also devised that allows deeper mixing in windier conditions. The YSU more accurately simulates deeper vertical mixing in buoyancy-driven PBLs with shallower mixing in strong-wind regimes compared to MRF, however it has still been found to over deepen the PBL for springtime deep convective environments, resulting in too much dry air near the surface and underestimation of Mixed Layer Convective Available Potential Energy (MLCAPE) related to environments of deep convection [21].

1.2.5 Microphysics parameterizations

Microphysics includes explicitly resolved water vapor, cloud, and precipitation processes. The model is general enough to accommodate any number of mass mixing-ratio variables, and other quantities such as number concentrations. Four-dimensional arrays with three spatial indices and one species index are used to carry such scalars. Memory, i.e., the size of the fourth dimension in these arrays, is allocated depending on the needs of the scheme chosen, and advection of the species also applies to all those required by the microphysics option. In the current version of the ARW, microphysics is carried out at the end of the time-step as an adjustment process, and so does not provide tendencies. The rationale for this is that condensation adjustment should be at the end of the time-step to guarantee that the final saturation balance is accurate for the updated temperature and moisture. However, it is also important to have the latent heating forcing for potential temperature during the dynamical sub-steps, and this is done by saving the microphysical heating as an approximation for the next time-step. WRF offers microphysics parameterization options with different level of sophistication:

- Warm rain (i.e., no ice) – Kessler (idealized) [22]
- Simple ice (3 arrays) – WSM3 [23]
- Mesoscale (5 arrays, no graupel) – WSM5 [23]
- Cloud-scale single-moment (6 arrays, graupel) – WSM6, Lin, Goddard, Eta-Ferrier [24]
- Double-moment (8-13 arrays) – Thompson, Morrison, WDM5, WDM6, NSSL [25]

Single-moment schemes have one prediction equation for mass (kg/kg) per species with particle size distribution being derived from fixed parameters.

Double-Moment (DM) schemes add a prediction equation for number concentration (#/kg) per DM species, bearing in mind that DM schemes may only be double-moment for a few species and that they allow for additional processes such as size-sorting during fall-out and sometimes aerosol (cloud condensation nuclei) effects.

Co-funded by the European Union
EUROPEAN PARTNERSHIP

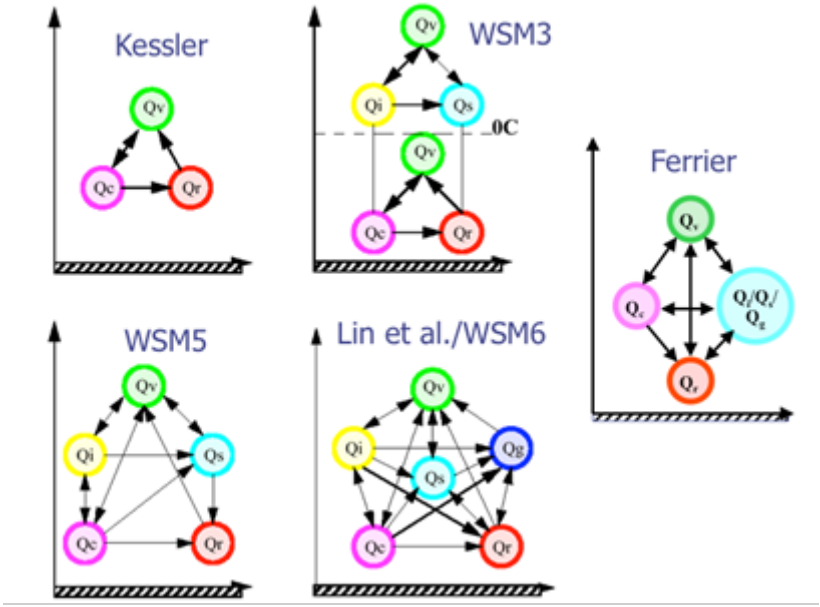

Figure 4: illustration of microphysics interactions for schemes with different level of sophistication, where Qv stands for water vapour, Qc for cloud water, Qr for rain water, Qi for cloud ice, Qs for snow, and Qg for graupel.

The scheme adopted in this project is the WSM6 which extends the WSM5 scheme to include graupel and its associated processes. Therefore, it includes water vapor, rain, snow, cloud ice, cloud water, and graupel. Some of the graupel-related terms follow [26], but its ice-phase behavior is much different due to the changes of [23]. A new method for representing mixed-phase particle fall speeds for the snow and graupel particles by assigning a single fall speed to both that is weighted by the mixing ratios and applying that fall speed to both sedimentation and accretion processes is introduced. The behavior of the WSM3, WSM5, and WSM6 schemes differ little for coarser mesoscale grids, but they work much differently on cloud-resolving grids. Of the three WSM schemes, the WSM6 scheme is the most suitable for cloud-resolving grids, considering the efficiency and theoretical backgrounds [27]. As a further step towards high-resolution applications WRF also supplies a double-moment version (WDM6) of this scheme for warm rain processes, so that cloud condensation nuclei, and number concentrations of cloud and rain are also predicted.

1.2.6 Radiation parameterizations

The radiation schemes provide atmospheric heating due to radiative flux divergence and surface downward longwave and shortwave radiation for the ground heat budget. Longwave radiation includes infrared or thermal radiation absorbed and emitted by gases and surfaces. Upward longwave radiative flux from the ground is determined by the surface emissivity that in turn depends upon land-use type, as well as the ground temperature. Shortwave radiation includes visible and surrounding wavelengths that make up the solar spectrum. Hence, the only source is the Sun, but processes include absorption, reflection, and scattering in the atmosphere and at surfaces. For shortwave radiation, the upward flux is the reflection due to surface albedo. Within the atmosphere the radiation responds to model-predicted cloud and water vapor distributions, as well as specified carbon dioxide, ozone, and (optionally) trace gas concentrations. All the radiation schemes in WRF currently are column (one-dimensional) schemes, so each column is treated independently, and the fluxes correspond to those in infinite horizontally uniform planes, which is a good approximation if the vertical thickness of the

Co-funded by the European Union
EUROPEAN PARTNERSHIP

model layers is much less than the horizontal grid length. This assumption would become less accurate at high horizontal resolution.

The radiation scheme adopted in this project is the Rapid Radiative Transfer Model for GCMs (RRTMG, [28]) which is a state-of-the-art widely used radiative model for weather and climate applications both globally and regionally. The schemes use spectral bands and the k-distribution method of integration with look-up tables for efficiency. For clouds with cloud fractions that vary vertically it uses the MonteCarlo Independent Column Approximation (MCICA) together with a maximum-random overlap assumption by default (random, maximum, exponential and exponential-random methods are also available). It can also make use of effective radii of cloud water, ice and snow if they come from the microphysics, or it will use its own assumptions if these are not provided. It includes the effect of trace gases and has an option for their time variation for climate projections. For ozone there is a global monthly climatology option. Aerosols can use a global monthly climatology [29], [30] or can come from optical properties computed by WRF-Chem or can be specified/input in other ways.

1.3 PhaSt algorithm

The Phase Stocastic (PhaSt [31]) algorithm is a spectral-based nowcasting procedure based on the empirical nonlinear transformation of precipitation fields provided by radar measurements and on the stochastic evolution of the transformed fields in spectral space. This procedure can provide an ensemble, probabilistic nowcasting of precipitation fields up to a lead time of few hours. In this approach, the initial one-point distribution and power spectrum of the precipitation field are kept constant, and a stochastic Ornstein–Uhlenbeck process [32] is used for the time evolution of the Fourier phases of the Gaussianized precipitation field. The method automatically includes large-scale advection of precipitation structures, and it reproduces the nonlinear and intermittent nature of rain fields. In addition, the use of spectral space instead of physical space assures that the spatial correlations of precipitation fields are preserved. The model requires two initial precipitation fields, to be used as initial conditions. It takes an empirical nonlinear transformation of the two precipitation fields used as initial conditions, $p(x,y,t=0)$ and $p(x,y,t=-\Delta t)$, generates two Gaussian fields, $g(x,y,0)$ and $g(x,y,-\Delta t)$. The Fourier transform of the Gaussianized fields are taken and their Fourier spectra, $\hat{g}(kx,ky,0)$ and $\hat{g}(kx,ky,-\Delta t)$, is obtained. From these for each wavenumber (kx,ky) the Fourier phase, ϕ, and an estimate of the Fourier angular frequency are calculated. Fourier phases are then evolved in time by a stochastic process while Fourier amplitudes are kept fixed. There are several stochastic models that can be used to evolve the Fourier phases. To allow for the presence of time correlations in the angular frequencies a Langevin-type model is used: the temporal evolution of the Fourier phase $\phi(kx,ky)$ at a given wavenumber (kx,ky) is written in terms of a linear Ornstein–Uhlenbeck stochastic process for the angular frequency. The Ornstein–Uhlenbeck process generates angular frequencies that have a Gaussian distribution with zero mean and variance σ^2 and an exponentially decaying temporal autocorrelation. The spectrum with the evolved Fourier phases is inverted to generate a nowcasted Gaussian field at the time t of interest, $g(x,y,t)$. This evolved field has the same power spectrum as the initial Gaussianized field, $g(x,y,0)$. Different realizations of the stochastic process allow for generating different evolutions of the precipitation field and for creating an ensemble of precipitation nowcasts. Then an inverse nonlinear transformation to pass from the evolved Gaussian field $g(x,y,t)$ to the nowcasted precipitation field is performed. The use of a stochastic process for the evolution of Fourier phases allows for generating many realizations, to be used as members of an ensemble of precipitation nowcasts. All ensemble members are characterized by the same amplitude

Co-funded by the European Union
EUROPEAN PARTNERSHIP

distribution and very similar power spectra. However, the phase evolution (i.e., the positioning of rainfall structures) evolves differently in the different realizations, providing an estimate of the probability of occurrence of precipitation at a given point in space and a given moment in time [33]. Since the probabilistic information are not suitable for the project, we used a deterministic approach by using the ensemble mean or some percentile. Moreover, the algorithm has been applied to the precipitation field, so firstly it was proved the feasibility of the approach in case of Vertical Integrated Liquid (VIL), Vertical Maximum Intensity (VIM) or VIL density (DVIL) defined as VIL/ETM where ETM is the cloud Echo Top in metre.

1.4 RaNDeVIL algorithm

The RaNDeVIL (Radar Nowcasting Density VIL) is a radar based nowcasting algorithm that extrapolates the future positions of potentially severe storms by its identification based on the 2D product Density of Vertical Liquid Integration (DVIL). The DVIL magnitude is a combination of the radar products Vertical integrated liquid (VIL) and Echo Top Maximum of 20 dBZ (ETM). The VIL is a weather radar measurement equivalent to the total amount of liquid water available in a vertical column of the atmosphere. High VIL values may indicate either large hail occurrence, large amounts of small hail, or very high rainfall intensity. The ETM is the maximum height at which the weather radar still receives reflectivity signal of 20 dBZ intensity (or higher). It is an estimation of the top of storm clouds. Then the DVIL product combines the VIL and ETM information, dividing the estimation of the liquid water in a vertical column of the atmosphere with the maximum height of the storm cloud development, becoming a good severe weather indicator with less dependency on seasonality [34]. The normalization of the length of the water column makes DVIL suitable to compare different convective storms occurred in different seasons of the year. It is a derived product described by eq. (1), not directly calculated by the weather radar software but very easy to obtain.

$$DVIL\ \left[\frac{kg}{m^3}\right] = \frac{VIL\left[\frac{kg}{m^2}\right]}{ETM[m]} \qquad \text{(eq. 1)}$$

Other works such those by [35] have already suggested the potential of VIL and ETM magnitudes to be helpful in ATM in route operations into the US in route operations.

RaNDeVIL is a three steps algorithm:

1) Convective activity detection and storm identification: after VIL and ETM digested and DVIL is computed the algorithm searches for storm structures exceeding the DVIL threshold of 1g/m^3 with a minimum extension of 10km^2. The minimum intensity threshold and size restriction are chosen according to the previous radar analysis of the different study cases (extended analysis over deliverable 5.1) and the characteristics of convective storms in the Mediterranean [36].

2) Tracking of storm cells: after the identification of all the active storms the affected areas are compared with the storms in the previous time step. If they are new storms, the structure is labelled with a numeric identification, the centroid of mass of the storm is computed and other information of different radar magnitudes are stored. On the contrary, if the structures already existed in the past, information of the previous time steps is recovered and the label assigned is the same that had in the past, allowing an easy tracking of the different positions of the storm centroid.

3) Nowcasting the future positions of the storms: If a storm has been observed at least twice in the last time steps, the nowcasting of the future positions storm centroid is computed for the

Co-funded by the European Union
EUROPEAN PARTNERSHIP

next 30min with 5min steps. The future position is estimated by calculating the motion vector of past scans using linear least squares, where the extrapolation of the storm area is computed assuming the conservation of the actual storm area (it is to say, the estimated area variation in the next 5 minutes is smaller than the 10% of the total storm area).

The algorithm outputs are different text files containing the positions of identified storms, the stored radar parameters as well as the nowcasted positions for the current storms. Additionally, the forecast of the affected areas for the next five to thirty minutes are stored in different shape files making it very easy to visualize the predicted evolution of the storms in the region of interest.

For its tracking capabilities, the algorithm must be running continuously, restarting the procedure each time that a new weather radar product is generated (every 5 minutes in the case of Italian weather radar). This is done to not lose the storm history that helps to improve the nowcasting procedure, the addition of new information every 5 minutes ensures the best performance of the algorithm. As the algorithm works with the radar data fields, the native spatial resolution RaNDeVIL is the same than the weather radar products, but it can be easily up scaled if necessary.

Even though it is simpler than other multilevel (3D) pure radar nowcasting algorithms or numerical nowcasting approaches, its potential ability to predict convective storms and its easy implementation on operative systems makes it worth it to test the algorithm for the study cases of SINOPTICA.

Co-funded by the European Union

EUROPEAN PARTNERSHIP

2 References

[1] Grell, G., L. Schade, R. Knoche, A. Pfeiffer, and J. Egger (2000). Nonhydrostatic climate simulations of precipitation over complex terrain, J. Geophys. Res., 105, 29,595–29,608

[2] Parodi, A., & Emanuel, K. (2009). A theory for buoyancy and velocity scales in deep moist convection. Journal of the Atmospheric Sciences, 66(11), 3449-3463.

[3] Parodi, A., & Tanelli, S. (2010). Influence of turbulence parameterizations on high-resolution numerical modeling of tropical convection observed during the TC4 field campaign. *Journal of Geophysical Research: Atmospheres*, *115*(D10).

[4] Parodi, A., Foufoula-Georgiou, E., & Emanuel, K. (2011). Signature of microphysics on spatial rainfall statistics. Journal of Geophysical Research: Atmospheres, 116(D14).

[5] Fiori, E., Comellas, A., Molini, L., Rebora, N., Siccardi, F., Gochis, D. J., & Parodi, A. (2014). Analysis and hindcast simulations of an extreme rainfall event in the Mediterranean area: The Genoa 2011 case. Atmospheric Research, 138, 13-29.

[6] Fiori, E., Ferraris, L., Molini, L., Siccardi, F., Kranzlmueller, D., & Parodi, A. (2017). Triggering and evolution of a deep convective system in the Mediterranean Sea: Modelling and observations at a very fine scale. Quarterly Journal of the Royal Meteorological Society, 143(703), 927-941.

[7] Pieri, A. B., von Hardenberg, J., Parodi, A., & Provenzale, A. (2015). Sensitivity of precipitation statistics to resolution, microphysics, and convective parameterization: A case study with the high-resolution WRF climate model over Europe. *Journal of Hydrometeorology*, *16*(4), 1857-1872.

[8] Lagasio, M., Silvestro, F., Campo, L., & Parodi, A. (2019a). Predictive capability of a high-resolution hydrometeorological forecasting framework coupling WRF cycling 3dvar and Continuum. Journal of Hydrometeorology, 20(7), 1307-1337.

[9] Lagasio, M., Parodi, A., Pulvirenti, L., Meroni, A. N., Boni, G., Pierdicca, N., & Rommen, B. (2019b). A synergistic use of a high-resolution numerical weather prediction model and high-resolution earth observation products to improve precipitation forecast. Remote Sensing, 11(20), 2387.

[10] Wicker, L. J., & Skamarock, W. C. (2002). Time-splitting methods for elastic models using forward time schemes. Monthly weather review, 130(8), 2088-2097.

[11] Paulson, C. A., (1970). The mathematical representation of wind speed and temperature profiles in the unstable atmospheric surface layer. J. Appl. Meteor., 9, 857–861.

[12] Dyer, A. J., and B. B. Hicks (1970). Flux-gradient relationships in the constant flux layer, Quart. J. Roy. Meteor. Soc., 96, 715–721.

[13] Beljaars, A.C.M., (1994). The parameterization of surface fluxes in large-scale models under free convection, Quart. J. Roy. Meteor. Soc., 121, 255–270.

[14] Zhang, D., & Anthes, R. A. (1982). A high-resolution model of the planetary boundary layer—Sensitivity tests and comparisons with SESAME-79 data. Journal of Applied Meteorology, 21(11), 1594-1609.

Co-funded by the European Union

EUROPEAN PARTNERSHIP

[15] Smirnova, T. G., J. M. Brown, and S. G. Benjamin, 1997: Performance of different soil model configurations in simulating ground surface temperature and surface fluxes. Mon. Wea. Rev., 125, 1870–1884.

[16] Smirnova, T. G., J. M. Brown, S. G. Benjamin, and D. Kim, 2000: Parameterization of cold season processes in the MAPS land-surface scheme. J. Geophys. Res., 105 (D3), 4077–4086.

[17] Hong, S.-Y., and Y. Noh, and J. Dudhia, (2006a). A new vertical diffusion package with an explicit treatment of entrainment processes. Mon. Wea. Rev., 134, 2318–2341.

[18] Hong, S.-Y., and H.-L. Pan, (1996) Nonlocal boundary layer vertical diffusion in a medium-range forecast model, Mon. Wea. Rev., 124, 2322–2339.

[19] Noh, Y., W.G. Cheon, S.-Y. Hong, and S. Raasch (2003). Improvement of the K-profile model for the planetary boundary layer based on large eddy simulation data. Bound.-Layer Meteor., 107, 401–427.

[20] Hong, S.-Y., 2007: Stable Boundary Layer Mixing in a Vertical Diffusion Scheme. The Korea Meteor. Soc., Fall conference, Seoul, Korea, Oct. 25-26.

[21] Coniglio, M.C., Correia, J., Marsh, P.T., Kong, F., 2013. Verification of convection-allowing WRF model forecasts of the planetary boundary layer using sounding observations. Weather Forecast. 28, 842–862. http://dx.doi.org/10.1175/WAF-D-12-00103.1.

[22] Kessler, E. (1969). On the distribution and continuity of water substance in atmospheric circulations. In On the distribution and continuity of water substance in atmospheric circulations (pp. 1-84). American Meteorological Society, Boston, MA.

[23] Hong, S.-Y., J. Dudhia, and S.-H. Chen (2004). A Revised Approach to Ice Microphysical Processes for the Bulk Parameterization of Clouds and Precipitation, Mon. Wea. Rev., 132, 103–120.

[24] Rogers, E., Black, T., Ferrier, B., Lin, Y., Parrish, D., & DiMego, G. (2001). National Oceanic and Atmospheric Administration Changes to the NCEP Meso Eta Analysis and Forecast System: Increase in resolution, new cloud microphysics, modified precipitation assimilation, modified 3DVAR analysis. NWS Tech. Proced. Bull, 488, 1-15.

[25] Mansell, E. R., Ziegler, C. L., & Bruning, E. C. (2010). Simulated electrification of a small thunderstorm with two-moment bulk microphysics. Journal of Atmospheric Sciences, 67(1), 171-194.

[26] Lin, Y.-L., R. D. Farley, and H. D. Orville, (1983) Bulk parameterization of the snow field in a cloud model. J. Climate Appl. Meteor., 22, 1065–1092.

[27] Hong, S.-Y., and J.-O. J. Lim, (2006b). The WRF Single-Moment 6-Class Microphysics Scheme (WSM6), J. Korean Meteor. Soc., 42, 129–151.

[28] Iacono, M. J., Delamere, J. S., Mlawer, E. J., Shephard, M. W., Clough, S. A., & Collins, W. D. (2008). Radiative forcing by long-lived greenhouse gases: Calculations with the AER radiative transfer models. Journal of Geophysical Research: Atmospheres, 113(D13).

[29] Tegen, I., Hollrig, P., Chin, M., Fung, I., Jacob, D., & Penner, J. (1997). Contribution of different aerosol species to the global aerosol extinction optical thickness: Estimates from model results. Journal of Geophysical Research: Atmospheres, 102(D20), 23895-23915.

Co-funded by the European Union

EUROPEAN PARTNERSHIP

[30] Thompson, G., & Eidhammer, T. (2014). A study of aerosol impacts on clouds and precipitation development in a large winter cyclone. Journal of the atmospheric sciences, 71(10), 3636-3658.

[31] Metta, S., von Hardenberg, J., Ferraris, L., Rebora, N., & Provenzale, A. (2009). Precipitation nowcasting by a spectral-based nonlinear stochastic model. Journal of Hydrometeorology, 10(5), 1285-1297.

[32] Uhlenbeck, G. E., & Ornstein, L. S. (1930). On the theory of the Brownian motion. Physical review, 36(5), 823.

[33] Poletti, M. L., Silvestro, F., Davolio, S., Pignone, F., and Rebora, N. (2019). Using nowcasting technique and data assimilation in a meteorological model to improve very short range hydrological forecasts, Hydrol. Earth Syst. Sci., 23, 3823–3841, https://doi.org/10.5194/hess-23-3823-2019.

[34] Edwards, R., & Thompson, R. L. (1998). Nationwide comparisons of hail size with WSR-88D vertically integrated liquid water and derived thermodynamic sounding data. Weather and Forecasting, 13(2), 277-285,p://dx.doi.org/10.1175/1520-0434(1998)013%3C0277:NCOHSW%3E2.0.CO;2

[35] Rubnich, M., & DeLaura, R. (2010). An algorithm to identify robust convective weather avoidance polygons in en route airspace. In 10th AIAA aviation technology, integration, and operations (ATIO) conference (p. 9164), https://doi.org/10.2514/6.2010-9164

[36] del Moral, A., Llasat, M. del C. and Rigo, T.: Connecting flash flood events with radar-derived convective storm characteristics on the northwestern Mediterranean coast: knowing the present for better future scenarios adaptation, Atmos. Res., 238(July), doi:10.1016/j.atmosres.2020.104863, 2020.

Co-funded by the European Union

EUROPEAN PARTNERSHIP